Design of a predictive targeting error simulator for MRI-guided prostate biopsy

Shachar Avni, Siddharth Vikal, Gabor Fichtinger
School of Computing, Queen's University, Kingston, ON, Canada

ABSTRACT

Multi-parametric MRI is a new imaging modality superior in quality to Ultrasound (US) which is currently used in standard prostate biopsy procedures. Surface-based registration of the pre-operative and intra-operative prostate volumes is a simple alternative to side-step the challenges involved with deformable registration. However, segmentation errors inevitably introduced during prostate contouring spoil the registration and biopsy targeting accuracies. For the crucial purpose of validating this procedure, we introduce a fully interactive and customizable simulator which determines the resulting targeting errors of simulated registrations between prostate volumes given user-provided parameters for organ deformation, segmentation, and targeting. We present the workflow executed by the simulator in detail and discuss the parameters involved. We also present a segmentation error introduction algorithm, based on polar curves and natural cubic spline interpolation, which introduces statistically realistic contouring errors. One simulation, including all I/O and preparation for rendering, takes approximately 1 minute and 40 seconds to complete on a system with 3 GB of RAM and four Intel Core 2 Quad CPUs each with a speed of 2.40 GHz. Preliminary results of our simulation suggest the maximum tolerable segmentation error given the presence of a 5.0 mm wide small tumor is between 4-5 mm. We intend to validate these results via clinical trials as part of our ongoing work.

Keywords: Segmentation, validation, error, modeling, prostate, cancer, MRI, biopsy.

1. INTRODUCTION

The definitive diagnostic method for detecting prostate cancer, the most common non-cutaneous cancer in men[1], is image-guided needle biopsy. Surprisingly, cancers as large as a sugar cube are routinely missed in standard trans-rectal Ultrasound (TRUS) biopsy procedures[2]. Multi-parametric MRI is a novel imaging modality offering superior soft tissue contrast and high spatial resolution, making it both a useful diagnostic and navigational tool. The procedure involves several hours of pre-operative imaging for the ultimate purpose of precisely determining the ideal biopsy target locations. During the intervention, the pre-operative images are spatially registered with newly acquired intra-operative images in real-time.

Differing patient positions (supine during planning and prone during intervention) make the registration difficult. Specifically, large anatomical misalignment and organ deformation necessitates a costly deformable registration. A simple and fast approach would be to segment the prostate in both images and apply surface-based registration. However, prostate segmentation is prone to errors, which spoil the registration accuracy and, ultimately, lead to targeting errors. It is not yet known how errors in segmentation affect intra-prostatic targeting errors.

It is possible that biopsy targets may be extracted successfully despite targeting inaccuracies. For instance, targeting errors that are less than the diameter of the needle tip (approximately 2.5 mm) are deemed clinically insignificant as they do not affect the extraction. The question is: when does segmentation error become large enough as to significantly affect the final targeting? To that end, the purpose of this work is to introduce a piece of software that determines the resulting targeting errors of simulated surface registrations when given parameters for organ deformation, segmentation, and targeting.

2. BACKGROUND

The current gold standard for image-guided prostate biopsy is TRUS[3]. TRUS-based procedures inherently rely on US images for needle guidance. Unfortunately, the soft-tissue contrast in US images is poor and cannot be used to locate

cancerous lesions. The work presented in this paper is the first stage in a validation study of MRI-guided prostate biopsy, an attractive alternative to TRUS currently undergoing clinical validation. This study aims to prove the reliability of the procedure in the presence of human error introduced in image segmentation. There have already been proof-of-concept studies for the procedure[4,5] as well as research into the partial automation of the prostate segmentation phase[6].

A similarly-motivated study has been undertaken by Kim et al.[7] where they validate a mutual information-based registration method for digitally reconstructed radiographs. They quantified the set-up error by recording the physical offsets of fiducial marker placements with the ground truth. Another study by Quarantelli et al.[8] introduces a method for increasing accuracy in the registration of PET and MRI brain images. The method was refined using simulations of PET scans with the introduction of increasingly larger experimental errors. Lastly, Wu and Zipes[9] investigate the relationship between segmentation errors and the resulting excitation parameters for cardiac membranes. Our work is the first to focus on quantifying the relationship between segmentation error and targeting accuracy in the MRI-guided prostate biopsy procedure.

3. METHODS

The main workflow of the simulator, shown in Fig. 1, begins with the generation of the ground truth pre-op prostate contour instantiated from a statistical shape atlas. The ground truth pre-op target points are then placed within the contour according to user-specified parameters. Deformation is then applied to the ground truth pre-op contour by means of a random deformation field simulating the change in organ shape between the time of pre-operative and intra-operative imaging. The resulting ground truth intra-op target points are then determined by applying the deformation field to the ground truth pre-op target points. Next, the two contours are segmented automatically and individually, with segmentation errors introduced by our segmentation error introduction algorithm. The segmented contours are then registered in deformable fashion, with the resulting deformation field applied to the ground truth pre-op target points generating the registered target points. Finally, the registered target points are compared with the ground truth intra-op target points and the targeting error statistics are recorded. The individual steps in the workflow are discussed in detail in this section.
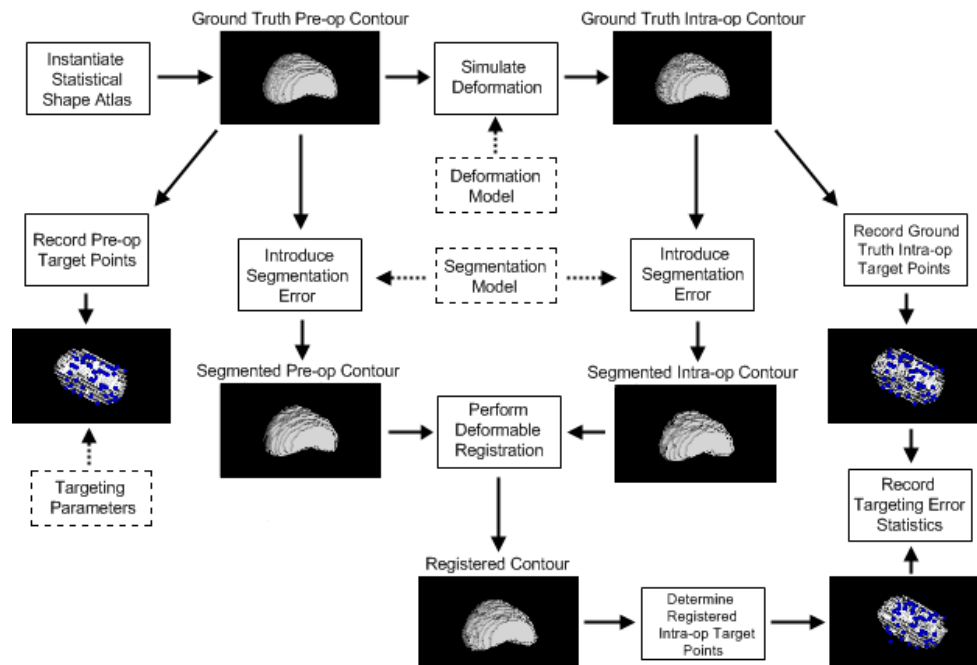

Figure 1.The workflow of one simulated surface registration between programmatically-generated prostate volumes as executed by the simulator.

3.1 Generation of 3D prostate contours with a statistical shape atlas

One main requirement of the simulator is the ability to run an infinite number of test cases given a finite number of input data. Using the method described by Tsai et al.[10], we obtain and align a set of 3D prostate contours, constructed from stacks of segmented axial slices and modeled as voxelized binary volumes. From this set, we obtain the mean shape, Φ, and three eigenshapes, σ_1, σ_2, and σ_3, using the technique developed by Leventon et al.[11]. We then generate three weights, w_1, w_2, and w_3, obtained randomly from within the corresponding eigen-value bounds. A statistical shape atlas creates a new contour, $C = \Phi + w_1\sigma_1 + w_2\sigma_2 + w_3\sigma_3$, at the beginning of the simulation.

3.2 Simulating deformation

The ground truth intra-op contour, representing the true geometry of the prostate during the intra-operative imaging phase, is created by applying a deformation field to the contour generated above. Deformation is randomly applied slice-wise to the surface of the prostate. Three parameters are set by the user for controlling the process: the probability of deformation, p, the minimum deformation magnitude in mm, m_d, and the maximum deformation magnitude in mm, M_d. Deformation proceeds at each extremal contour pixel of each slice with probability p as follows: Determine the vector leading from the centroid of the axial section of the prostate contained in the slice to the current pixel i, transform this vector to metric space and normalize it. Call this vector V_c. Obtain a random number, r, between m_d and M_d, and generate the vector V_v by transforming rV_c to pixel space. Then, with probability of inversion 0.5, invert V_v, and call this final vector V_f. Compute the discretized path from the current pixel i, to the pixel $i + V_f$ using Bresenham's line algorithm[12]. If this path points towards the centroid of the slice, remove each pixel corresponding to the prostate along the path. Otherwise, create new pixels corresponding to the prostate along the path. This algorithm deforms an input contour with random forces applied parallel to the axial plane towards (or from) the centroid of each image slice. Example outputs obtained from running this algorithm on a particular contour can be seen in Fig. 2.
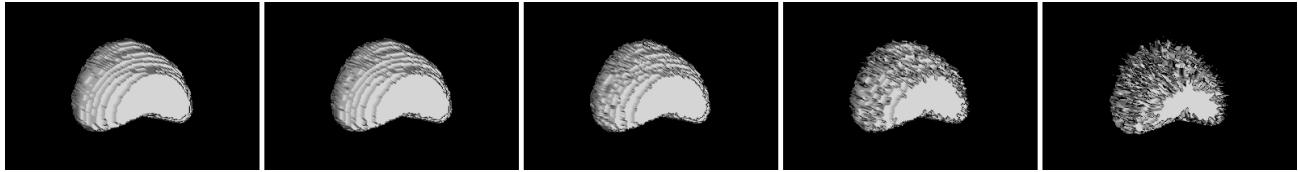

Figure 2. Sample outputs obtained from our deformation algorithm. From left to right with parameters (p, md, Md): original contour, (0.25, 0.5 mm, 1 mm), (0.5, 0.5 mm, 2 mm), (0.5, 1 mm, 4 mm), (0.75, 2 mm, 8 mm).

3.3 Introduction of segmentation error

The ground truth contours are segmented slice-wise as follows: Separate the axial section of the prostate in the current slice into N radial segments (Fig. 3 a). Mark the extremal pixels where the rays at the boundaries of the segments intersect the surface of the prostate as $\{S_1, S_2, \ldots, S_N\}$. Let c be the centroid of the axial section of the prostate contained in the slice. For each pixel S_i, determine the offset vector v with endpoints (c, S_i). Compute the pixel S_i' some random distance d_i between d_{min} and d_{max} (in millimeters) away from S_i along v (with probability 0.5, use the vector $-v$ instead) (Fig. 3 b). Convert each S_i' to polar coordinates (r_i, Θ_i) with respect to c. Next, determine the curve $\zeta: \Theta \rightarrow r$ using natural cubic spline interpolation between the points (r_i, Θ_i) taking r as a function of Θ (Fig. 3 c). This curve ζ, with points (r, Θ) transformed to Cartesian coordinates and plotted in pixel space, represents a smooth segmentation of the input contour with accuracy determined by the parameters N, d_{min}, and d_{max} (Fig. 3 d).

The segmentation algorithm introduced above offsets each pixel S_i from the surface of the contour independently. This is unattractive as it may result in fluctuations in the contours which would not appear in sketches by a real physician. To remedy this, two more parameters are introduced: the parameter M, which is the minimum amount of pixels S_i to be perturbed before the offset vector switches signs, and the parameter D, which is the maximum allowable difference between the current offset distance d_i and the previous offset distance d_{i-1}. Moreover, there are different values for the parameter pair (d_{min}, d_{max}) for the base, mid, and apex regions, allowing each individual region a different level of contouring certainty. Fig. 4 shows the smoothing effects of the parameters M and D when the algorithm is applied using the same values of N, d_{min}, and d_{max}.
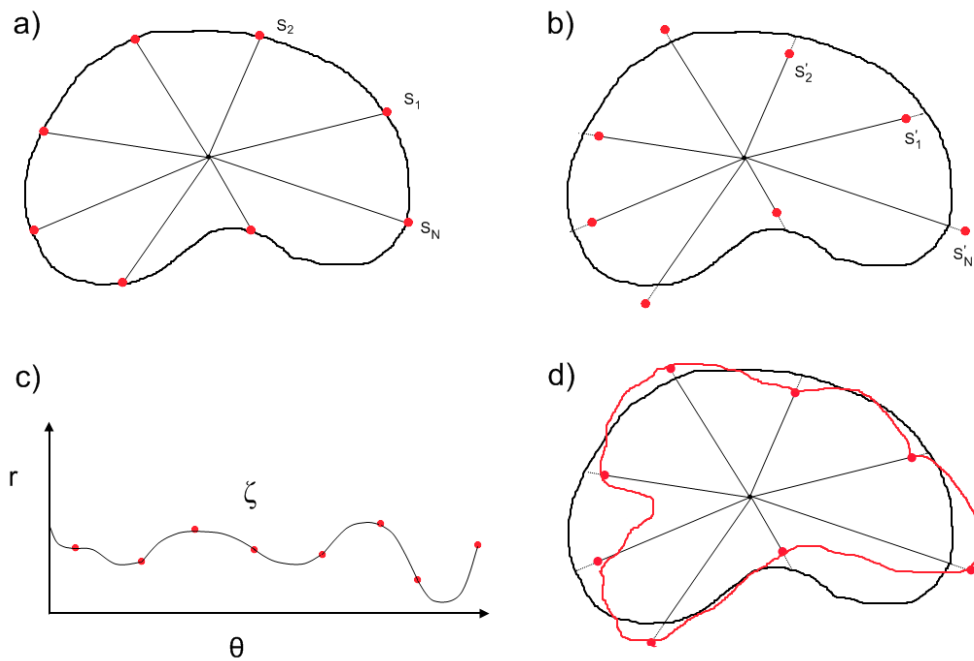
Figure 3. Workflow of the segmentation error introduction algorithm. a) Axial MRI slice separated into N radial segments b) Perturbed segment endpoints c) Natural cubic spline interpolation of the endpoints transformed into polar coordinates d) Curve resulting from transformation of spline interpolation to voxel space
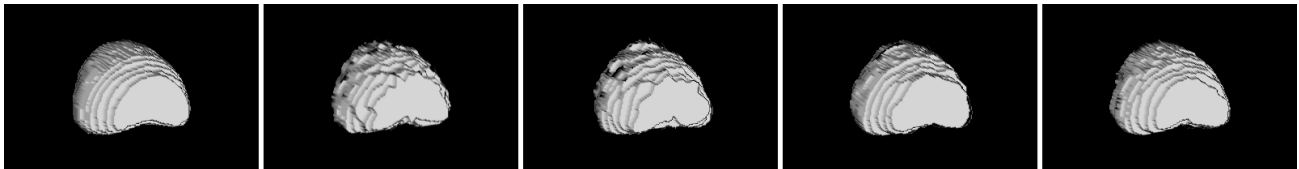

Figure 4. Contours obtained after running our segmentation error introduction algorithm. From left to right with parameters (M, D): original contour, $(1, \infty)$, $(2, 0.5\ mm)$, $(4, 0.3\ mm)$, $(8, 0.2\ mm)$. All instances were run with $N = 31$, $(d_{min}, d_{max})_{apex} = (0\ mm, 2.5\ mm)$, $(d_{min}, d_{max})_{mid} = (0\ mm, 1\ mm)$, and $(d_{min}, d_{max})_{base} = (0\ mm, 2.5\ mm)$.

3.4 Targeting parameters and targeting error

The ideal biopsy locations are placed on the ground truth pre-op contour according to user-specified parameters. There are two targeting schemes in the current version of the simulator: (1) target points are placed systematically in the peripheral zone of the prostate (systematic targeting), or, (2) target points are placed in all locations reachable by a needle using the trans-rectal MRI-guided manipulator employed in our procedure (global targeting).

For the systematic approach, the user specifies the number of biopsy regions along the left-right and inferior-superior axes. For instance, if the user selects 2 regions along the left-right axis and 3 regions along the inferior-superior axis, then the targeting method approximates the classical sextant biopsy scheme originally popularized by Hodge et al.[13]. The user also specifies a percentage, P, indicating the height of the peripheral zone with respect to the overall height of the prostate volume.

For the global targeting, all points are targeted except those falling in a slice-wise radial sweep of angle Θ (inputted by the user) centered on the anterior side of each slice's centroid. The area contained in this sweep approximates the fibro-muscular tissue on the anterior side of the urethra which is not targeted during the procedure. The user also selects
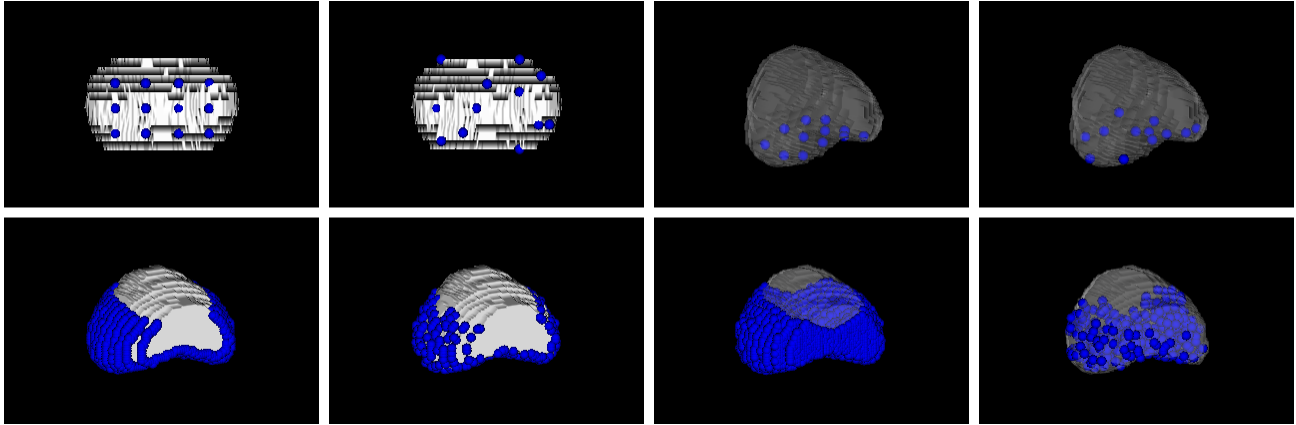
Figure 5. Summary of the possible targeting methods implemented in the simulator. Top: systematic targeting with 4 regions along the left-right axis and 3 regions along the inferior-superior axis and $P = 25\%$. From left to right: surface targeting, randomized surface targeting, regular targeting, randomized regular targeting. Bottom: global targeting with $\Theta = 120°$. From left to right: surface targeting, randomized surface targeting (25%), regular targeting, randomized regular targeting (1%).

whether the targeting is to be randomized and whether or not the target points are to be confined to the surface of the prostate. If random global targeting is chosen, the user also inputs the percentage of target points to be selected. A random systematic targeting places each target point in a random location in its corresponding biopsy region whereas systematic targeting alone places each target in the midpoint of the region. Fig. 5 displays a summary of the simulator's possible targeting methods.

After registration, the targeting error for each target point is calculated by finding the Euclidean distance between the registered and ground truth target points. Targeting error statistics, including minimum error, maximum error, mean error, mean deviation, and standard deviation are reported at this time.

3.5 Simulator output

Upon completion of the simulation, a screen summarizing the results and the parameters used is displayed for the user. All prostate volumes are displayed, including those without deformation as well as the volumes showing the difference with the ground-truth. This screen also displays the percentage of targeting errors that were significant and insignificant. The threshold values for insignificant and significant targeting errors are selected by the user. Fig. 6 is an example of the simulator's summary screen.

Finally, the simulator outputs a 3D color-coded heat map which visually summarizes the magnitudes of the targeting errors. On the map, green represents clinically insignificant error (i.e. ≤ 2.5 mm), red represents significant error (e.g. ≥ 5.0 mm) and errors in between are represented via a smooth color gradient. The user may run multiple simulations. If so, each voxel on the heat map represents the mean error over all simulations. Fig. 7 shows two views of a particular heat map outputted by the simulator.

The output of the simulation may be used to answer a number of queries on the relationship between segmentation error and targeting accuracy. The main query the simulator was designed to answer is "what is the maximum tolerable segmentation error for the procedure?" The maximum tolerable segmentation error would be the threshold where the targeting errors reach unacceptable proportions. To answer this query, set the threshold for significant error to be the maximum tolerable targeting error. This value would be set to, for example, the radius of the suspected cancer tumor. Next, the simulator would be run with differing segmentation parameters. The maximum segmentation error inputted in this fashion with the resulting targeting errors in acceptable range would be the maximum tolerable segmentation error. We ran this workflow on our simulator with the results summarized in section 4.

Weight mode 1: -0.07 Sigma
Weight mode 2: +0.85 Sigma
Weight mode 3: +0.01 Sigma
Base Segmentation Error: Uniform Random on [0 mm, 2.5 mm]
Mid Segmentation Error: Uniform Random on [0 mm, 2.5 mm]
Apex Segmentation Error: Uniform Random on [0 mm, 2.5 mm]

Total Targets: 1893
Total Insignificant (<= 0.5 mm): 1096 (57.9%)
Total Significant (>= 5.0 mm): 31 (1.6%)
Min Error: 0 mm
Max Error: 6.4 mm
Mean Error: 0.9 mm
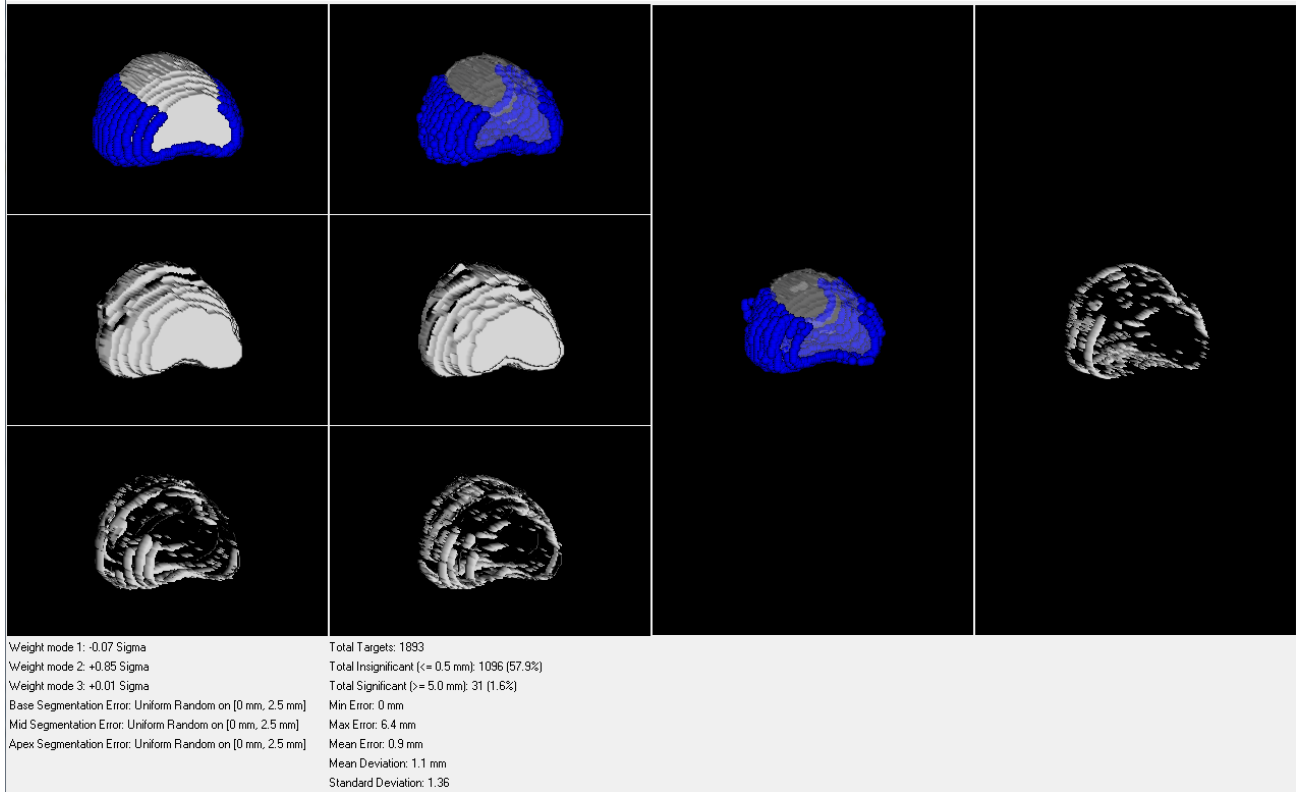Mean Deviation: 1.1 mm
Standard Deviation: 1.36

Figure 6. Simulation summary screen. Images in first column from top to bottom: ground-truth pre-op, pre-op with segmentation error, difference between pre-op and ground-truth pre-op. Images in second column from top to bottom: ground-truth intra-op, intra-op with segmentation error, difference between intra-op and ground-truth intra-op. Image in third column: contour resulting from registration with targeting points. Image in fourth column: difference between resulting contour and the ground-truth intra-op contour. This example was run with global surface targeting with $\Theta = 120°$.
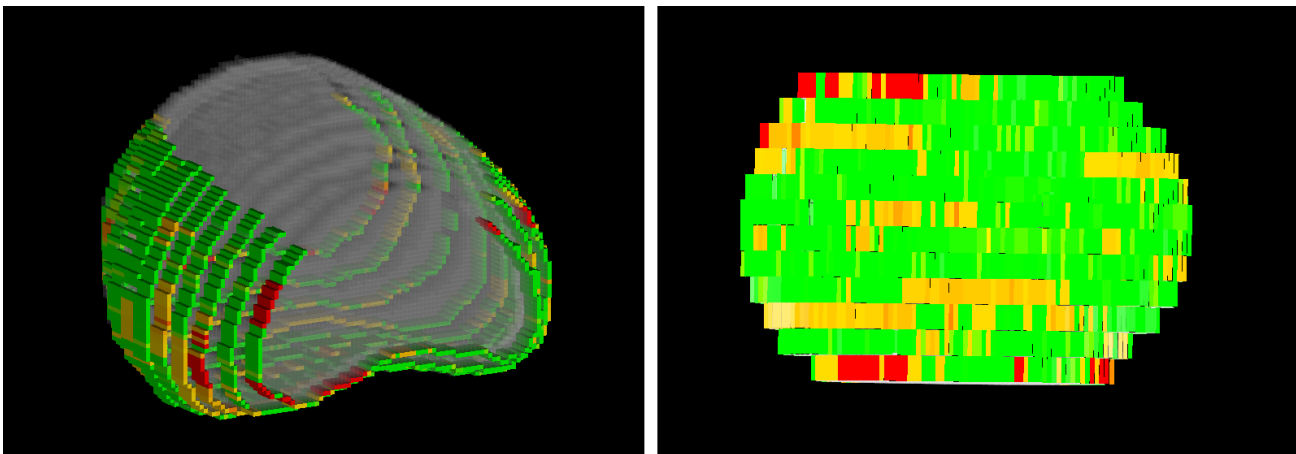

Figure 7. Two views of one outputted heat map. Threshold for insignificant error was set to 0.5 mm and the threshold for significant error was set to 5.0 mm. The simulation was run with global surface targeting with $\Theta = 120°$. Left: Side view (near side is the apex). Right: Inferior view (top is the apex, bottom is the base).

4. RESULTS AND DISCUSSION

The simulator has been implemented in C++ using Kitware's Insight Segmentation and Registration Toolkit (ITK) for image processing with the Visualization Toolkit (VTK) and KWWidgets used for display. The simulation is fully automated and takes approximately 1 minute and 40 seconds to complete on a system with 3 GB of RAM and four Intel Core 2 Quad CPUs each with a speed of 2.40 GHz. Simulations were run with increasing values of d_{max} with global surface targeting ($\Theta = 120°$), deformation parameters $\{p = 0.25, m_d = 0.5$ mm, $M_d = 2.0$ mm$\}$ and segmentation parameters $\{N = 31, M = 5, D = 0.5$ mm$\}$, with $d_{min} = 0$ mm for all three regions of the prostate. The threshold for insignificant error was set to be less than or equal to 2.5 mm (the diameter of the needle tip) and the threshold for significant error was set to be greater than or equal to 5.0 mm (representing the width of a small tumor). The frequency of significant error in targeting reached unacceptable rates ($> 10\%$) with values for d_{max} at approximately 4.8 mm suggesting the maximum tolerable segmentation error, given the existence of a tumor with a 5.0 mm width, is between 4-5 mm. These results should be validated with segmentation and deformation parameters obtained via clinical trials.

Future work includes incorporating the ability for the user to select and move target points in a 3D view. Other work includes improving the deformation method with the implementation of a simplified FEM-based deformation model based on current techniques[14]. The simplification of the model is due to the fact that important physical parameters such as boundary constraints[15] are not yet known for the prostate with great confidence. The segmentation method will be improved by means of an observational study which will include the gathering of multiple physician-segmented prostate contours. These contours would then be used as inputs to a PCA model where the resulting atlas would generate the segmented contours themselves.

We have presented the framework for a fully interactive and customizable simulator which is able to plausibly predict the resulting targeting errors in an MRI-guided prostate biopsy procedure given specific segmentation, organ deformation and targeting parameters. We have described the algorithms used in detail, including an algorithm which introduces statistically realistic segmentation errors. Preliminary results, based on the confines of our deformation and segmentation models, suggest the maximum tolerable segmentation error given the presence of a small tumor of width 5.0 mm is between 4-5 mm. When given clinically-produced segmentation and deformation models obtained in future work, the simulator may be used to determine the true correlation between segmentation error and targeting accuracy.

REFERENCES

[1] Jemal, A. et al., "Cancer statistics, 2008," CA 58(2), 71-96 (2008).
[2] Anastasiadis, A. G. et al., "MRI-guided biopsy of the prostate increases diagnostic performance in men with elevated or increasing PSA levels after previous negative TRUS biopsies," European Urology 50(4), 738-749 (2006).
[3] Eisenberg, M. L., Cowan, J. E., Davies, B. J., Caroll, P. R., and Shinohara K., "The importance of tumor palpability and transrectal ultrasonographic appearance in the contemporary clinical staging of prostate cancer," Urologic Oncology: Seminars and Original Investigations, In Press, Corrected Proof, Available online (2009).
[4] Fichtinger, G. et al., "Transrectal Prostate Biopsy Inside Closed MRI Scanner with Remote Actuation, under Real-Time Image Guidance," Proc. MICCAI 2488, 91-98 (2002).
[5] Susil, R. C. et al., "Transrectal prostate biopsy and fiducial marker placement in a standard 1.5T magnetic resonance imaging scanner," The Journal of Urology 175(1), 113-120 (2006).
[6] Vikal, S., Haker, S., Tempany, C., and Fichtinger, G., "Prostate contouring in MRI guided biopsy," Proc. SPIE 7259, 72594A, (2009).
[7] Kim, J., Fessler, J. A., Lam, K. L., Balter, J. M., and Ten Haken, R. K., "A feasibility study on mutual information based set-up error estimator for radiotherapy," Medical Physics 28(12), 2507-2517 (2001).
[8] Quarantelli et al., "Integrated software for the analysis of brain PET/SPECT studies with partial-volume-effect correction," Journal of Nuclear Medicine 45(2), 192-201 (2004).
[9] Wu, J. and Zipes, D. P., "Effects of spatial segmentation in the continuous model of excitation propagation in cardiac muscle," Journal of Cardiovascular Electrophysiology 10(7), 965-972 (2007).
[10] Tsai, A. et al., "A shape-based approach to the segmentation of medical imagery using level sets," IEEE Trans. on Medical Imaging 22(2), 137-154 (2003).

[11] Leventon, M. E., Grimson, W. E. L., and Faugeras, O., "Statistical shape influence in geodesic active contours," Proc. the IEEE Computer Society Conference on Computer Vision and Pattern Recognition, 316-323 (2000).
[12] Bresenham, J. E., "Algorithm for computer control of a digital plotter," IBM Systems Journal 4(1), 25-30 (1965).
[13] Hodge, K. K., McNeal, J. E., Terris, M. K., and Stamey, T. A., "Random systematic versus directed ultrasound guided transrectal core biopsies of the prostate," The Journal of Urology 142(1), 71-75 (1989).
[14] Goksel, O., Salcudean, S.E. and DiMaio, S.P., "3D simulation of needle-tissue interaction with application to prostate brachytherapy," Computer Aided Surgery, in press.
[15] Misra, S., Macura, K. J., Ramesh, K. T. and Okamura, A. M., "The importance of organ geometry and boundary constraints for planning of medical interventions," Medical Engineering & Physics 31(2), 195-206 (2009).